(12)

SECURITY CLASS.

AD-A265 217

DOCUMENTATION PAGE

1a REPORT S Unclassified	1b RESTRICTIVE MARKINGS
2a SECURITY CLASSIFICATION AUTHORITY	3. DISTRIBUTION / AVAILABILITY OF REPORT
2b DECLASSIFICATION / DOWNGRADING SCHEDULE	Unlimited Distribution
4 PERFORMING ORGANIZATION REPORT NUMBER(S)	5. MONITORING ORGANIZATION REPORT NUMBER(S)
6a NAME OF PERFORMING ORGANIZATION UCLA, Electrical Engineering 6b OFFICE SYMBOL (If applicable)	7a NAME OF MONITORING ORGANIZATION Naval Research Laboratory
6c ADDRESS (City, State, and ZIP Code) 405 Hilgard Avenue, Los Angeles, CA 90024	7b ADDRESS (City, State, and ZIP Code) Code 6840 Naval Research Laboratory Washington, D.C. 20375
8a NAME OF FUNDING / SPONSORING ORGANIZATION Office of Naval Research 8b OFFICE SYMBOL (If applicable)	9 PROCUREMENT INSTRUMENT IDENTIFICATION NUMBER Contract No. N00014-87-K-2032
8c ADDRESS (City, State, and ZIP Code) 800 N. Quincy St., Arlington, VA 22217	10 SOURCE OF FUNDING NUMBERS PROGRAM ELEMENT NO / PROJECT NO / TASK NO / WORK UNIT ACCESSION NO

11. TITLE (Include Security Classification)

Slow Wave Cyclotron Autoresonance Masers

12 PERSONAL AUTHOR(S)
N.C. Luhmann, Jr. and D.B. McDermott

13a TYPE OF REPORT	13b TIME COVERED	14 DATE OF REPORT (Year, Month, Day)	15 PAGE COUNT
Final Technical Report	FROM 10/87 TO 5/91	July 9, 1991	

16. SUPPLEMENTARY NOTATION

17. COSATI CODES			18 SUBJECT TERMS (Continue on reverse if necessary and identify by block number)
FIELD	GROUP	SUB-GROUP	

19. ABSTRACT (Continue on reverse if necessary and identify by block number)

93 5 20 083

MAY 8 1993

20 DISTRIBUTION / AVAILABILITY OF ABSTRACT	21 ABSTRACT SECURITY CLASSIFICATION
☒ UNCLASSIFIED/UNLIMITED ☐ SAME AS RPT ☐ DTIC USERS	Unclassified
22a NAME OF RESPONSIBLE INDIVIDUAL Dr. Y.S. Park	22b TELEPHONE (Include Area Code) / 22c OFFICE SYMBOL

Final Technical Report

(1) Contract Title: Slow Wave Cyclotron Autoresonance Masers

Number: N00014-87-K-2032

Principal Investigator: Dr. N.C. Luhmann, Jr.
Department of Electrical Engineering
University of California, Los Angeles
56-147N ENG-IV
Los Angeles, CA 90024
Tel: (213) 825-4163

Program Manager: Dr. Y.S. Park

(2) Technical Objectives:

To conduct experimental and theoretical investigations of microwave generation based on the highly efficient cyclotron resonant maser (CRM) concept.

(3) Approach:

Electromagnetic coupling of a gyrating electron beam with an electromagnetic wave having a phase velocity near the speed of light was theoretically and experimentally investigated. For this value of phase velocity, the electrons remain in synchronism even as they lose energy, yielding high efficiency operation. Also, the frequency is upshifted by a factor of $(1\text{-}\beta_{\|})^{-1}$ over the gyrotron. Two approaches were pursued. In our conventional fast wave CARM, high beam voltage together with a moderately high perveance combine to produce extremely high power. In our dielectric loaded CARM, the waves are retarded such that a low energy electron beam can access the efficient autoresonant region. We also investigated using dielectric loading to dramatically widen the bandwidth of gyro-TWTs.

In the negative energy CRM, a negative energy cyclotron wave with resonance, $\omega = -\Omega_c + k_{\|}v_{\|}$, couples to a positive energy, slow waveguide mode. Since the beam mode is a negative energy wave, an initial transverse velocity is not required for wave growth. We have investigated employing dielectric loaded waveguide as the slow wave structure.

To provide frequency selective feedback for these microwave generation schemes, Bragg reflectors were developed. A Bragg reflector, which consists of corrugated waveguide, will reflect a wave whose axial wavelength is twice the corrugation period.

(4) Accomplishments During Fourth Quarter CY 90 (October 1, 1987 - March 31, 1991)

A. Dielectric Loaded CARM

1. Experiment

The experiment was designed as an oscillator. A beam with a voltage of 75-100 kV and a velocity ratio of, α = 0.6 - 1.5 was employed to interact with a wave near the light line. To optimize the interactions in both the wiggler region and the CARM region, the solenoid for each region was controlled independently. By sweeping the axial magnetic field of the CARM solenoid and hence moving the cyclotron resonance line along the dispersion curve of the wave, several axial modes in the cavity were excited including a gyro-BWO at up to 24.6 kW and a gyrotron with emission of 12.8 kW, as shown in Fig. 1. Of much interest is that a wave of $k_{||} = 0.7\ (\omega/c)$ was excited at 12.72 GHz with a power of 300 W and a Doppler upshift of 44%. This mode was inaccurately reported initially as having $k_{||} = 1.06\ (\omega/c)$.

The low interaction efficiency near the light line and the inability to excite a mode on the light line can be accounted for by the relatively high axial velocity spread of the electron beam. It has been shown that a high quality electron beam ($\Delta v_{||}/v_{||} \leq 2\%$) is required for efficient CARM interaction. In our electron gun configuration, the dominant source of velocity spread is the transverse inhomogeneity of the wiggler's field. A diagnostic experiment was performed to examine the performance of the gyroresonant velocity transformation in the wiggler. Using an aperture, an extremely thin beam was passed through the wiggler and impacted on a fluorescent Uranium glass plate, so that the Larmor radius of the electrons could be measured and the α could be determined. The experimental results are shown in Fig. 2 and are consistent with simulation where a linear taper of the wiggler's amplitude was assumed.

Figure 3 shows the competition behavior of the excited modes, which happen to be even order axial HE_{11} modes. It shows that mode competition does <u>not</u> seem to be occurring. As the magnetic field is varied, one mode shuts off as the next turns on, which is desirable. However, it is a problem that only the even order modes are excited, since they are very weakly externally coupled. It is the odd modes which are strongly coupled out. This probably explains why our output power has been so low. The intercavity power is actually much higher. The saturation measurements shown in Fig. 4 reveal uncommon behavior. The power of a saturated gyrotron usually remains constant as the electron beam current is increased. However, the output power level of our device falls precipitously as the current increases, which may indicate that the velocity spread of our corkscrew beam increases with increasing space charge.

2. Simulation

By mid-1990, we had begun simulating the CARM interaction in the dielectric loaded rectangular waveguide shown in Fig. 5 as proposed by A.K. Ganguly for the Slow Wave Cyclotron Amplifier in order to avoid the TE/TM cross terms of the actual HE_{11} mode in cylindrical waveguide. The rationale for this was to find the optimum operating parameters for a CARM in a dielectric loaded structure, which was more amenable to analysis. The advantage of this structure is that its LSE_{10} mode, which is very similar to the unloaded

TE_{10} mode in rectangular waveguide, is generally well behaved and is the lowest order mode for both the fast and slow wave region.

Unfortunately, we have found very little evidence of efficient autoresonant interaction in the rectangular dielectric loaded CARM. Using the self-consistent particle tracing traveling-wave simulation code written by our student K.C. Leou, Fig. 6 shows the behavior of the interaction as the gyroresonance line intersects the slow waveguide mode near the vacuum light-line ($\beta_{ph} = 1$), where the autoresonance condition is satisfied. Figure 6(a) shows that the efficiency falls precipitously as the light-line is approached, even though the interaction becomes more autoresonant as shown in Fig. 6(b), i.e., the change in the Doppler-shift term more nearly compensate the change in the cyclotron frequency. (Here, and throughout these figures, the cyclotron frequency shift and the Doppler shift are shown at the point where the cyclotron frequency shift reaches a maximum). The problem is that the beam is not bunching strongly and this is due to autoresonance. Thus, autoresonance is seen as having a negative effect on efficiency. A finite velocity spread will exacerbate the low efficiency even further.

We became suspicious that perhaps an efficient CARM intrinsically could not be achieved with a low energy electron beam. Therefore, we decided to study low energy CARMs in plain unloaded waveguide, in which high energy CARMs are known to yield high theoretical efficiency. The uncoupled dispersion diagram of the gyro-interaction in rectangular waveguide (TE_{10}) is shown in Fig. 7. We are neglecting the secondary problems such a device would pose, such as the backward wave interaction. As the magnetic field is increased, the forward wave interaction becomes more autoresonant. Figure 8(a) shows that the efficiency of a high energy electron beam ($\approx$ 750 kV) increases as $\omega \rightarrow \infty$ ($\beta_{ph} \rightarrow 1$). Figure 9(a) with a higher α ($\alpha = v_\perp / v_\parallel$) also shows this, but to a lesser degree, since high α electrons do not maintain autoresonance as well. However, the same behavior as before is found for 100 kV electrons: Figs. 8(b) and 9(b) show that autoresonance is well maintained (the two resonance shift terms compensate each other almost perfectly) for the case closer to the light-line, while Figs. 8(a) and 9(a) show that the efficiency is worse for the autoresonant case. The parameter which is most strongly correlated with high efficiency is the magnitude of the change in either the cyclotron frequency or the Doppler shift (compare Fig. 8(a) with Figs. 8(b) and 8(c) and Fig. 9(a) with Figs. 9(b) and 9(c)), rather than the cancellation of one term by the other (autoresonance). A large change in the Doppler shift term is indicative of strong bunching.

Figure 10 shows the dependence of efficiency on α for V_0 = 100 kV and $\omega \gg \omega_c$. It is seen that the efficiency can be improved for higher α, but this is not due to increased autoresonance. Again, higher efficiency is strongly correlated with changes in the Doppler shift, but not correlated to its compensation by a change in the cyclotron frequency.

Figure 11(a) shows that the efficiency of a 100 kV beam is almost maximum for an initial mismatch of zero where the mismatch is defined as $\Delta = (\omega - \Omega_c - k_\parallel v_\parallel)/\omega$ when $\omega >> \omega_c$ (represented by ω= 5.36). A gyrotron (represented by ω = 3.36) is seen to yield higher efficiency for a larger mismatch. However, in either case, it is seen from Figs. 11(b) and (c) that autoresonance is independent of mismatch. The mismatch value of $\Delta = 0$ has been used for all of the other figures.

In Fig. 12(a), a small amount of autoresonant enhancement of the efficiency may be evident for a beam current of 10A. As the operating frequency is raised above the cutoff, the efficiency increases somewhat. Figure 12(c) shows that autoresonance becomes more complete as ω is raised above ω_c. The efficiency enhancement may or may not be due to autoresonance, but it is sufficiently small to be ignored. The case with I = 50A in Fig.

12(a) does not display any autoresonant efficiency enhancement.

In summary, autoresonance does not lead to tight bunch formation for low energy electrons and therefore tends to yield lower efficiency. This was found using an unloaded fast waveguide. There is no reason to think that the situation will improve for a dielectric loaded guide. Therefore, the only advantage of using dielectric in the waveguide is to achieve a reasonable frequency upshift ($\approx (1-\beta_{\|})^{-1}$) with a low energy beam.

B. Dielectric Loaded Wideband Gyro-TWT

Although we have not yet observed autoresonance in simulations of the slow waveguide shown in Fig. 5, this structure has been used in an extremely important new device. Wideband operation of a fast wave gyro-TWT has been numerically demonstrated. Our self-consistent simulation code has found that an instantaneous bandwidth of 20% can be achieved which is to be compared with a conventional gyro-TWT's typical bandwidth of 5%. Dr. Ganguly has shown that an instantaneous bandwidth as high as 30% can be obtained in a Slow Wave Cyclotron Amplifier (SWCA), in which the interaction circuit is also represented by Fig. 5. However, the SWCA has also been shown to be very sensitive to the axial velocity spread of the beam, since the interaction occurs for $\omega/ck_z < 1$ and therefore the wave has a large propagation constant k_z.

The drawback of the SWCA can be avoided while still retaining the advantage of broad bandwidth if the interaction can be made to occur in the fast wave region where the wave has a relatively small propagation constant. To achieve a bandwidth comparable with that of a SWCA, a low α ($= v_{\perp}/v_z$) electron beam and a moderate dielectric constant ($\epsilon_r \sim 5$) are most appropriate, since the interaction range of frequency is proportional to the slope of the waveguide/beam mode. The dispersion characteristic of a typical dielectric loaded waveguide is shown in Fig. 13, where the light line ($\omega = kc$) and the beam line ($\omega = k_z v_z + \Omega_{co}/\gamma$) are also given. It can be seen that the grazing condition can be approximately maintained in the fast wave region for a frequency range corresponding to an instantaneous bandwidth of 30-40%.

We have used the simulation code for the dielectric loaded CARM to design a high performance amplifier. Table 1 lists the parameters for a broadband Ka-band gyro-TWT. In Fig. 14, the saturation efficiency is plotted as a function of frequency for several values of axial velocity spread. For an ideal beam, a saturation efficiency of 22% and a potential bandwidth of 32% can be obtained. It can also be seen that interaction in the high frequency region is more susceptible to electron beam quality as a result of the larger propagation constant.

To obtain the instantaneous bandwidth, efficiency is plotted as a function of frequency by fixing the interaction length at $L/a = 120$, which was determined based on results from Fig. 14. As shown in Fig. 15, the instantaneous bandwidth falls from 25% for $\Delta v_z/v_z = 0.0\%$ to 20% for $\Delta v_z/v_z = 2\%$. The peak efficiency obtained (10-15%) is lower than for a conventional gyro-TWT or a SWCA. However, standard efficiency enhancement techniques, such as a depressed collector to recover the unused energy of the low α beam, can be employed to improve its performance.

The student K.C. Leou designed a single anode MIG gun which can produce an electron beam appropriate for the Dielectric Loaded Wideband Gyro-TWT. The design is similar to the gun in K.R. Chu's successful gyro-TWT at NTHU. The parameter's are listed in Table 2 and Fig. 16 shows the magnetic field profile and electron trajectories from Herrmannsfeldt's EGUN simulation code. The velocity spread is predicted to be $\Delta v_{\|}/v_{\|} = 2\%$. A MIG with

this design is currently being fabricated.

C. Bragg Reflectors

Our development of Bragg reflectors for overmoded, frequency selective cavities, including sinusoidal and rectangular corrugation, culminated in the design of tapered corrugation with a Hamming-Window distribution. We received our two Hamming-Window Bragg reflectors for our HV CARM from the electroformer, A.J. Tuck, and measured their reflectivity and transmission with an automated network analyzer. As can be seen in Figs. 17 and 18, the measurements are in excellent agreement with the predictions of the designer, Prof. M. Thumm of Stuttgart University, who used his scattering matrix code to simulate these improved reflectors which exhibit high mode purity. Figure 17 shows the measured and theoretical reflectivity of the upstream Bragg reflector, whose high reflectance of 99.6% was chosen in order to protect the CARM's gun from high rf flux. The measured and theoretical reflectivity of the downstream output Bragg section with a reflectance of 96% is shown in Fig. 18. We have also measured the Q of our HV CARM's Bragg cavity consisting of these two Hamming-Window reflectors and a smooth resonator section. The experimental data are shown in Fig. 19 along with the theoretical prediction of $Q = k^2 L / \left[k_{\|} (1 - R_1 R_2)\right]$.

D. HV CARM

We have collaborated with Drs. Caplan and Kulke of LLNL on the development of a high power 250 GHz CARM oscillator utilizing UCLA's high field superconducting solenoid and driven by a 2 MV, 2 GW induction linac. Multimegawatt, broadband superradiant emission was observed with a heterodyne receiver while using a single section 250 GHz, TE_{11} cylindrical Bragg cavity. Although frequencies greater than 230 GHz were observed using a cutoff filter, the Bragg cavity was not excited in the TE_{11} mode. It may have been excited in a higher order mode. We supplied LLNL with a calibrated high power FIR calorimeter, several back-up, broadband, robust detectors, high and low frequency mixers with accompanying heterodyne amplifier systems, the overmoded waveguide runs for both the 250 GHz output and the competing 25 GHz output at the interaction tube's cutoff, and helped to calibrate their diffraction tank.

The 400 kV UCLA CARM has also been partially assembled. It will use the 99.4% and 96% Hamming Window Bragg reflectors which were recently fabricated and tested. The beam pipe has been designed and the high voltage modulator has been fired into a nonlinear load by using it to drive a SLAC XK5 klystron.

E. Negative Energy CRM

We have also begun theoretical investigations of a completely new cyclotron resonance maser concept with tremendous potential. A negative energy cyclotron wave with resonance condition, $\omega = -\Omega_c + k_{\|} v_{\|}$, will couple to a positive energy, slow waveguide mode with a growth rate which can be even larger than the space charge mode for intense ($\omega_p/\omega \geq 0.1$), high voltage ($\gamma \geq 2$) electron beams. Since the beam mode is a negative energy wave, an initial transverse velocity is not required for wave growth. The free energy for wave growth derives from the axial streaming motion of the electron beam. All electrons in a cold beam follow the same trajectory relative to the wave. Wave trapping does not determine saturation. Efficiencies of 30% have been found through simulation. Furthermore, this interaction is fairly insensitive to the electron beam's velocity spread.

The slow waveguide mode must possess both transverse electric and magnetic fields. The transverse rf magnetic field modulates and bends the electrons into the transverse direction and the transverse rf electric field then absorbs the beam's transverse energy. We have investigated using dielectric to slow the guided wave. The suggested geometry is to propagate an electron beam along the center of a rectangular waveguide with dielectric slabs along the two narrow walls as shown in Fig. 5, because the TE_{10}-like mode is then the lowest order mode in both the fast and slow wave regions.

For the parameters of the proof of principle experiment described in Table 3, the growth rate of the negative energy cyclotron wave is seen in Fig. 20 to be greater than for the lower frequency space charge wave. It can be seen in Fig. 21 that this interaction is relatively immune to axial velocity spread in the beam.

(5) Significance

Our simulations did not find evidence of autoresonant enhancement of the efficiency near the light-line for low energy electrons in a dielectric loaded CARM nor even in an unloaded fast wave CARM with an elevated magnetic field. Rather, we found that autoresonance tends to lower the efficiency because it hinders bunch formation.

However, we found that a very broadband gyro-TWT can be obtained from the same dielectric loaded waveguide as used for the slow wave CARM. An instantaneous bandwidth of 20% can be achieved by loading a waveguide with dielectric to reduce its dispersion. This is a significant improvement over the conventional gyro-TWT's instantaneous bandwidth of only several percent. However, it was found that the dielectric loaded gyro-TWT requires a high quality electron beam with an axial velocity spread of $\Delta v_{\|}/v_{\|} \leq 2\%$. Fortunately, since the electron's α $(= v_{\perp}/v_{\|})$ is only 0.6, it is fairly straightforward to create such a beam.

Using Herrmannsfeldt's EGUN simulation code, we have designed a single anode MIG gun which produces an electron beam with an axial velocity spread of only $\Delta v_{\|}/v_{\|} = 2.7\%$ for $\alpha = 0.6$. The MIG is appropriate to drive the very wideband dielectric loaded gyro-TWT amplifier we developed in the previous period.

Bragg reflectors, which can provide selective feedback for overmoded oscillators, have been further optimized by tapering their amplitude. By fabricating and then measuring the reflectivity of a pair of Hamming-Window tapered Bragg reflectors, we verified the exciting computational predictions of M. Thumm. A resonator with these two Hamming-Window reflectors was measured to have a Q of 3000 for a frequency bandwidth of 10%.

The LLNL 2 MV TE_{11} CARM on which we are collaborating has undergone its initial phase of testing. Although high power (> 1 MW) was generated at high frequency (> 230 GHz), the rf is not due to excitation of the Bragg cavity's TE_{11} mode. The device with a single section Bragg reflector is acting like a superradiant amplifier, able to amplify at cyclotron harmonics as well as at the fundamental.

In the negative energy CRM, very high efficiency can be obtained due to the coupling of a positive energy electromagnetic mode to a negative energy cyclotron resonance beam mode. We believe the negative energy cyclotron wave will be to future high power microwave tubes what the negative energy space charge wave has been to communication TWTs.

(6) Listing (10/1987 - 5/1991)

"A Cherenkov Cyclotron Autoresonance Maser," D.B. McDermott, Haibo Cao and N.C. Luhmann, Jr., *Int. J. Electronics*, **65**, 477 (1988).

"CARM Amplifier Designs for High Power," Q.S. Wang, D.B. McDermott, A.T. Lin, N.C. Luhmann, Jr., K.R. Chu, A.Salop and M. Caplan, submitted for publication, *Int. J. of Infrared and Millimeter Waves*, **12**, 297 (1991).

"Initial Operation of a Cherenkov Cyclotron Autoresonance Maser," H. Cao, D.B. McDermott and N.C. Luhmann, Jr., *1988 IEEE Int. Conf. Plasma Science*, Seattle, Washington, 1988.

"Cyclotron Autoresonant Maser (CARM) EC Heating Source for High Field Tokamaks," Q.S. Wang, A.T. Lin, N.C. Luhmann, Jr., D.B. McDermott and K.R. Chu, *Bull. APS*, **33**, 2085 (1988).

"Initial Operation of a Cherenkov CARM," H.B. Cao, D.B. McDermott and N.C. Luhmann, Jr., *APS Bulletin* **33**, 2083 (1988).

"CARM EC Heating Source for High Field Tokamaks," Q.S. Wang, A.T. Lin, N.C. Luhmann, Jr., D.B. McDermott and K.R. Chu, *Digest of Thirteenth Int. Conf. IR & Mm-Waves*, Honolulu, Hawaii, 1988.

"Initial Operation of a Cherenkov CARM," H.B. Cao, D.B. McDermott and N.C. Luhmann, Jr., *Proceedings of Thirteenth Int. Conf. IR and mm-Wave*, Honolulu, Hawaii (1988).

"Initial Operation of a Cherenkov CARM," H.B. Cao, D.B. McDermott and N.C. Luhmann, Jr., *Proceedings of SPIE Conf. on Microwave and Particle Beam Sources and Directed Energy Concepts*, SPIE 1061, 248 (1989).

"Cyclotron Autoresonant Maser (CARM) EC Heating Source for High Field Tokamaks," Q.S. Wang, A.T. Lin, N.C. Luhmann, Jr., D.B. McDermott and K.R. Chu, *Proceedings of SPIE's Conf. on Microwave and Particle Beam Sources and Directed Energy Concepts*, SPIE 1061, 254 (1989).

"Design of a Bragg Resonator," C.K. Chong, D.B. McDermott, Mark Razeghi and N.C. Luhmann, Jr., *Digest of Fourteenth Int. Conf. on Infrared and Millimeter Waves*, Wurzburg, West Germany, 1989.

"Slowed Wave CARM," K.C. Leou, D.B. McDermott, and N.C. Luhmann, Jr., *Digest of Fourteenth Int. Conf. on Infrared and Millimeter Waves*, Wurzburg, West Germany, 1989.

"High Power CARM," Q.S. Wang, A.T. Lin, N.C. Luhmann, Jr., *Digest of Fourteenth Int. Conf. on Infrared and Millimeter Waves*, Wurzburg, West Germany, 1989.

"A Dielectric Loaded CARM," K.C. Leou, D.B. McDermott and N.C. Luhmann, Jr., *Bulletin of the American Physical Society* **34**, 2088 (1989).

"Design of a Bragg Resonator," C.K. Chong, D.B. McDermott, M. Razeghi and N.C. Luhmann, Jr., *Bulletin of the American Physical Society* 34, 2089 (1989).

"High Power CARM," Q.S. Wang, A.T. Lin, N.C. Luhmann, Jr., D.B. McDermott and K.R. Chu, *Bulletin of the American Physical Society* 34, 2089 (1989).

"Cyclotron Autoresonance Maser Amplifiers and Oscillators," Q.S. Wang, C.S. Kou, K.C. Leou, C.K. Chong, D.B. McDermott, A.T. Lin, N.C. Luhmann, Jr., M. Caplan, B. Kulke, A. Salop and K.R. Chu, *Digest of 1989 IEDM Conference.*

"Bragg Resonator for Selective Feedback in Overmoded Oscillators," C.K. Chong, M.M. Razeghi, D.B. McDermott, N.C. Luhmann, Jr., M. Caplan, and B. Kulke, *1990 SPIE Conf. on High Power Microwaves and Particle Beams*, SPIE 1226, p. 228, Los Angeles, California, 1990.

"High Power CARM for High Gradient RF Linac," Q.S. Wang, D.B. McDermott, A.T. Lin, N.C. Luhmann, Jr. and K.R. Chu, *1990 SPIE Conf. on High Power Microwaves and Particle Beams*, SPIE 1226, p. 220, Los Angeles, California, 1990.

"High Power CARM Amplifier," N.C. Luhmann, Jr., *1990 Microwave Power Tube Conf.*, Monterey, CA 1990.

"Bragg Resonator for Selective Feedback in Overmoded Oscillators," C.K. Chong, M.M. Razeghi, D.B. McDermott, and N.C. Luhmann, Jr., *IEEE Int. Conf. on Plasma Science*, Oakland, CA 1990.

"High Power CARM for High Gradient RF Linac," Q.S. Wang, D.B. McDermott, A.T. Lin, N.C. Luhmann, Jr. and K.R. Chu, *IEEE Int. Conf. on Plasma Science*, Oakland, CA 1990.

"Dielectric Loaded CARM," K.C. Leou, D.B. McDermott, N.C. Luhmann, Jr., *IEEE Int. Conf. on Plasma Science*, Oakland, CA 1990.

"Bragg Reflectors: Sinusoidal versus Rectangular Corrugation," C.K. Chong, D.B. McDermott, M.M. Razeghi, N.C. Luhmann, Jr., M. Thumm and J. Pretterebner, *SPIE Conf. Digest 15th International Conf. on Infrared and Millimeter Waves*, **1514**, 1990, pgs. 314a-314c.

"Negative Energy Cyclotron Resonance Maser," E.E. Lednum, D.B. McDermott, A.T. Lin and N.C. Luhmann, Jr., *SPIE Conf. Digest 15th International Conf. on Infrared and Millimeter Waves*, **1514**, 1990, pgs. 514-516.

"Dielectric Loaded Wideband Gyro-TWT," K.C. Leou, D.B. McDermott and N.C. Luhmann, Jr., *SPIE Conf. Digest 15th International Conf. on Infrared and Millimeter Waves*, **1514**, 1990, pgs. 687-689.

"CARM Design for Heating High Field Tokamak," Q.S. Wang, D.B. McDermott and N.C. Luhmann, Jr., *SPIE Conf. Digest 15th International Conf. on Infrared and Millimeter Waves*, **1514**, 1990, pgs. 690-692.

"Negative Energy Cyclotron Resonance Maser," E.E. Lednum, D.B. McDermott, A.T. Lin and N.C. Luhmann, Jr., *Digest of 1990 Int. Electron Devices Meeting*, **CH2865-4/90**, 1990, pgs. 707-710.

"Dielectric Loaded Broadband Gyro-TWT," K.C. Leou, D.B. McDermott and N.C. Luhmann, Jr., *Digest of 1990 Int. Electron Devices Meeting*, **CH2865-4/90**, 1990, pgs. 711-714.

"Bragg Reflectors: Tapered and Untapered," C.K. Chong, M.M. Razeghi, D.B. McDermott, N.C. Luhmann, Jr., M. Thumm and J. Pretterebner, *Digest of 1991 SPIE Conf. on Beams and High Power Microwaves.*

"Magnetically Tapered CARM for High Power," Q.S. Wang, D.B. McDermott and N.C. Luhmann, Jr., *Digest of 1991 SPIE Conf. on Beams and High Power Microwaves.*

"Negative Energy Cyclotron Resonance Maser," E.E. Lednum, D.B. McDermott, A.T. Lin and N.C. Luhmann, Jr., *Digest of 1991 SPIE Conf. on Beams and High Power Microwaves.*

"Bragg Reflectors: Sinusoidal versus Rectangular," C.K. Chong, D.B. McDermott, M.M. Razeghi, N.C. Luhmann, Jr., and M. Thumm, *1990 APS Plasma Physics Meeting*, Cincinnati, Ohio, 1990.

"Optimization of Magnetic Field Taper for CARM," Q.S. Wang, G. Vasilakos, D.B. McDermott, and N.C. Luhmann, Jr., *1990 APS Plasma Physics Meeting*, Cincinnati, Ohio, 1990.

"Low Voltage CARM with Dielectric Loading," K.C. Leou, D.B. McDermott, and N.C. Luhmann, Jr., *1990 APS Plasma Physics Meeting*, Cincinnati, Ohio, 1990.

"Negative Energy Cyclotron Resonance Maser," E. E. Lednum, D.B. McDermott, A.T. Lin and N.C. Luhmann, Jr., *1990 APS Plasma Physics Meeting*, Cincinnati, Ohio, 1990.

(8) Participants:

N.C. Luhmann, Jr., (P.I.)

D.B. McDermott (Co-P.I.)

K.C. Leou (Graduate Student)

H.B. Cao (Graduate Student)

FIGURE CAPTIONS

Figure 1. Results of initial operation of the Dielectric Loaded CARM. The dots represent the cold test measurements of the modes. The circles signify modes excited by the electron beam as the magnetic field was varied.

Figure 2. Magnetic field dependence of velocity ratio, $\alpha = v_\perp/v_\parallel$, produced by the gyroresonant wiggler. The solid line represents simulation results and the points denote measured data.

Figure 3. Dependence of start of oscillation current on magnetic field.

Figure 4. Dependence of output power on beam current.

Figure 5. Cross sectional view of dielectric loaded rectangular waveguide. Dashed line represents typical electrical field profile.

Figure 6. (a) Dependence of efficiency on frequency normalized to the frequency at which $\omega/ck_\parallel = 1$ for two values of beam current. The variance of relativistic gyrofrequency and Doppler shift for (b) I = 10 A and (c) I = 100 A. ($\omega_c = 1.57$, $\epsilon = 9.67$, b/a = 0.75, d/a = 0.75, $v_o = 100$ kV, $\Delta = 0.0$, $\alpha = 1.0$, $\Delta v_z/v_z = 0.0\%$.)

Figure 7. Uncoupled dispersion diagram of gyro-TWT with an elevated magnetic field showing the intersection of the gyroresonance line with a fast waveguide mode.

Figure 8. (a) Dependence of efficiency on beam voltage for $\alpha = 0.5$ and two values of frequency. The variance of relativistic gyrofrequency and Doppler shift for (b) $\omega = 5.36$ and (c) $\omega = 3.36$. ($\omega_c = 1.57$, $I_o = 50$ A, $P_{in} = 1$ kW, $\Delta = 0.0$, $\Delta V_z/v_z = 0.0\%$.)

Figure 9. (a) Dependence of efficiency on beam voltage for $\alpha = 1.0$ and two values of frequency. The variance of relativistic gyrofrequency and Doppler shift for (b) $\omega = 5.36$ and (c) $\omega = 3.36$. ($\omega_c = 1.57$, $I_o = 50$ A, $P_{in} = 1$ kW, $\Delta = 0.0$, $\Delta v_z/v_z = 0.0\%$.)

Figure 10. (a) Dependence of efficiency on $\alpha(= v_\perp/v_\parallel)$ for two values of beam current. The variance of relativistic gyrofrequency and Doppler shift for (b) $I_o = 50$ A and (c) $I_o = 10$ A. ($\omega_c = 1.57$, $V_o = 100$ kV, $\omega = 5.36$, $\Delta = 0.0$, $\Delta v_z/v_z = 0.0\%$.)

Figure 11. (a) Dependence of efficiency on mismatch ($\Delta = (\omega - \Omega_c - k_z v_z)/\omega$) for two values of frequency. Variance of gyrofrequency and Doppler shift for (b) $\omega = 5.36$ and (c) $\omega = 3.36$. ($\omega_c = 1.57$, $V_o = 100$ kV, $I_o = 10$ A, $\alpha = 1.0$, $\Delta v_z/v_z = 0.0\%$, $P_{in} = 100$ W.)

Figure 12. (a) Dependence of efficiency on frequency normalized to the cutoff frequency for two values of beam current. Variance of gyrofrequency and Doppler shift for (b) $I_o = 50$ A and (c) $I_o = 10$ A ($\omega_c = 1.57$, $V_o = 100$ kV, $\alpha = 1.0$, $\Delta = 0.0$, $\Delta v_z/v_z = 0.0\%$.)

Figure 13. Dispersion of dielectric loaded waveguide (solid line), cyclotron resonance line (dashed line) and vacuum light line (dotted line).

Figure 14. Dependence of saturation efficiency on frequency for several values of axial velocity spread for parameters listed in Table 1, except length is variable.

Figure 15. Dependence of instantaneous efficiency on frequency for several values of axial velocity spread for fixed parameters listed in Table 1.

Figure 16. Magnetic field profile and trajectories of electron beam from single anode magnetron injection gun as predicted by EGUN.

Figure 17. Frequency dependence of TE_{11} and TM_{11} mode reflection from a single Hamming-Window reflector with a peak corrugation amplitude of 0.40 cm from (a) scattering matrix simulation and (b) measurement. The input wave is in the TE_{11} mode.

Figure 18. Frequency dependence of TE_{11} and TM_{11} mode reflection from a single Hamming-Window reflector with a peak corrugation amplitude of 0.325 cm from (a) scattering matrix simulation and (b) measurement. The input is in the TE_{11} mode.

Figure 19. Theoretical and measured dependence of quality factor of Bragg resonator comprised of a 23.5 cm smooth section and the two Hamming-Window reflectors described in Figs. 17 and 18.

Figure 20. Dependence of growth rate on axial wavevector of negative energy cyclotron wave (SWCM) and space charge wave (SWCM) for proposed experiment described in Table 3, but with cold electron beam. ($\gamma = 2$, $\epsilon = 12$, $B_o = 3.6$ kG, and $\omega_p = 10^{10}$ rad /sec.

Figure 21. Dependence of efficiency from simulation for the proposed Negative Energy CRM proof of principle experiment described in Table 3.

Table 1. Design Parameters for Proposed Dielectric Loaded Broadband Gyro-TWT Proof of Principle Experiment.

Beam Voltage	100 kV
Beam Current	5 A
Center Frequency	10 GHz
Instantaneous Bandwidth	20 %
Output Power	40 - 80 kW
Gain	26-29 dB
Magnetic Field	3.0 kG
$v_\perp / v_z$	0.59
$\Delta v_z / v_z$	2.0 %
Interaction Length	90 cm
Waveguide Width	1.588 cm
Waveguide Height	1.111 cm
Dielectric Thickness	2.3 mm
Dielectric Constant	6.8

Table 2. Parameters of Magnetron Injection Gun with Single Anode for X-Band Dielectric Loaded Wideband Gyro-TWT.

Voltage	100 kV
Current	5 A
Current Density	6.75 A/cm^2
Angle of Emitting Surface	67°
Emitting Strip Radius	4.30 mm
Emitting Strip Length	2.63 mm
Cathode Anode Distance	3.53 cm
Magnetic Compression Ratio	4.5
Velocity Ratio	0.59
Axial velocity Spread	2.7 %
Guiding Center Spread	32 %

Table 3. Parameters for Proposed Negative Energy CRM Proof of Principle Experiment.

Beam Voltage	511 kV
Beam Current	68 A
Efficiency	27%
Frequency	9.3 GHz
Bandwidth	7%
Magnetic Field	3.6 kG
$\Delta v_{\|\|}/v_{\|\|}$	2.5%
Beam Radius	0.22 cm
Waveguide Broad Wall	1.2 cm
Waveguide Narrow Wall	0.436 cm
Dielectric Slab Thickness	0.382 cm
Dielectric Constant, ϵ	12

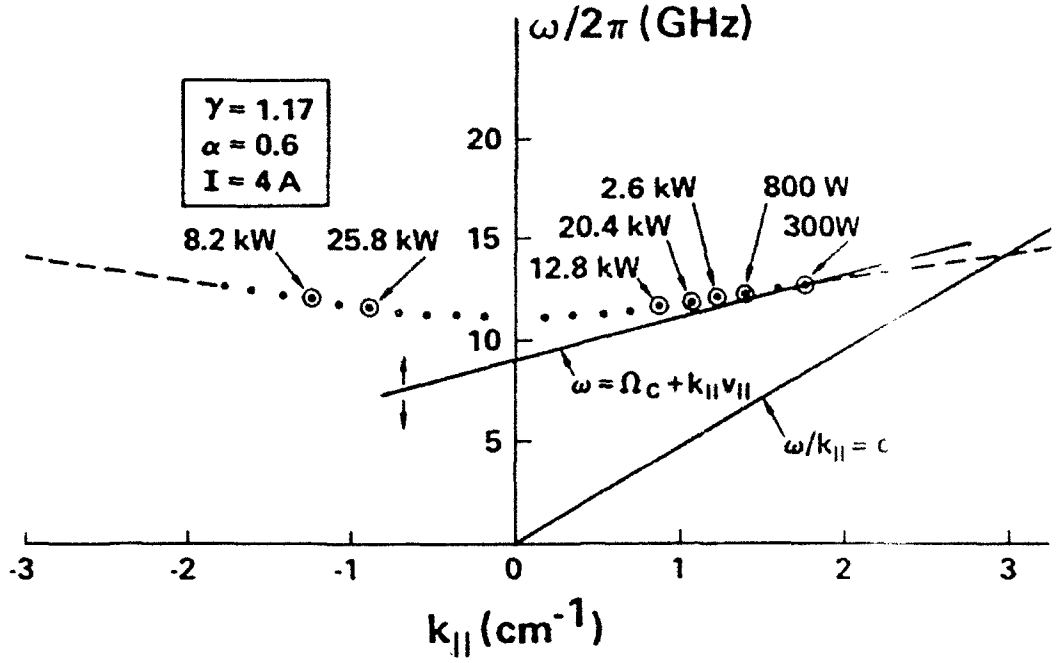

Figure 1. Results of initial operation of the Dielectric Loaded CARM. The dots represent the cold test measurements of the modes. The circles signify modes excited by the electron beam as the magnetic field was varied.

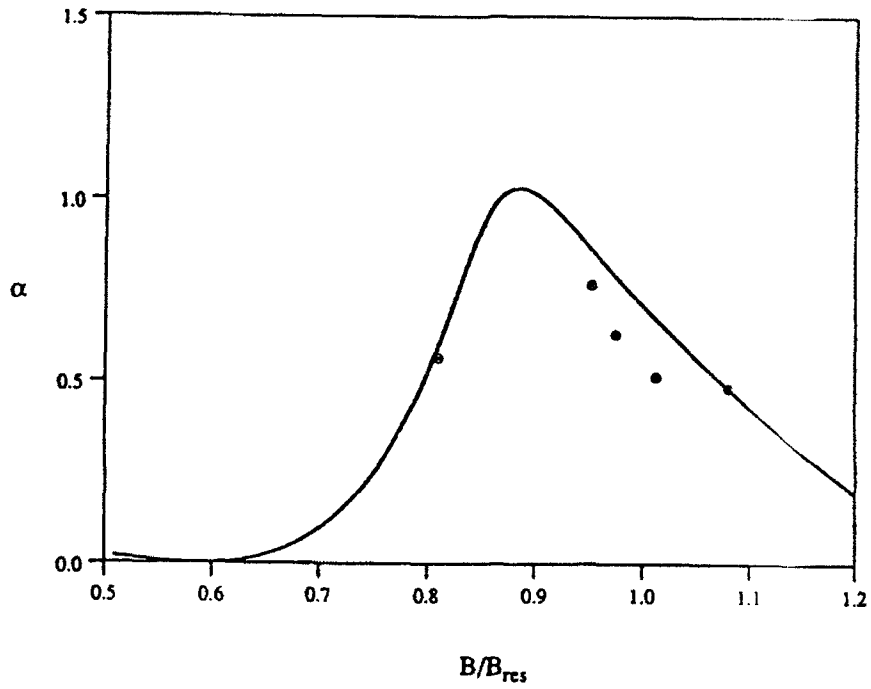

Figure 2. Magnetic field dependence of velocity ratio, $\alpha = v_\perp / v_\parallel$, produced by the gyroresonant wiggler. The solid line represents simulation results and the points denote measured data.

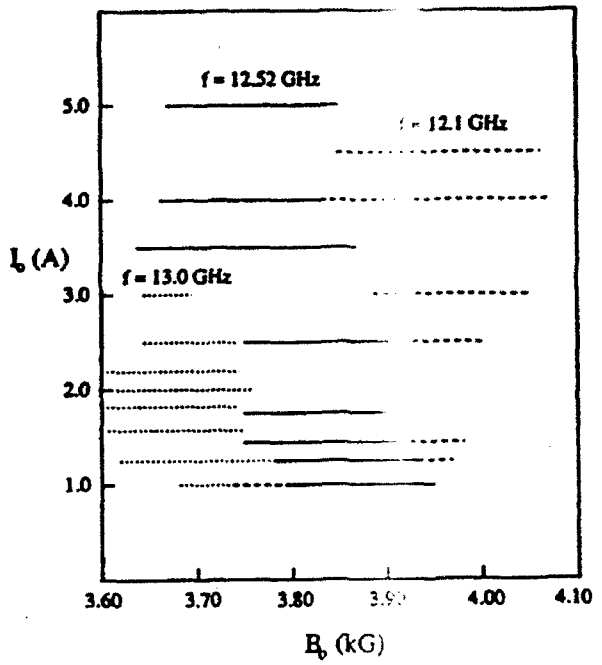

Figure 3. Dependence of start of oscillation current on magnetic field.

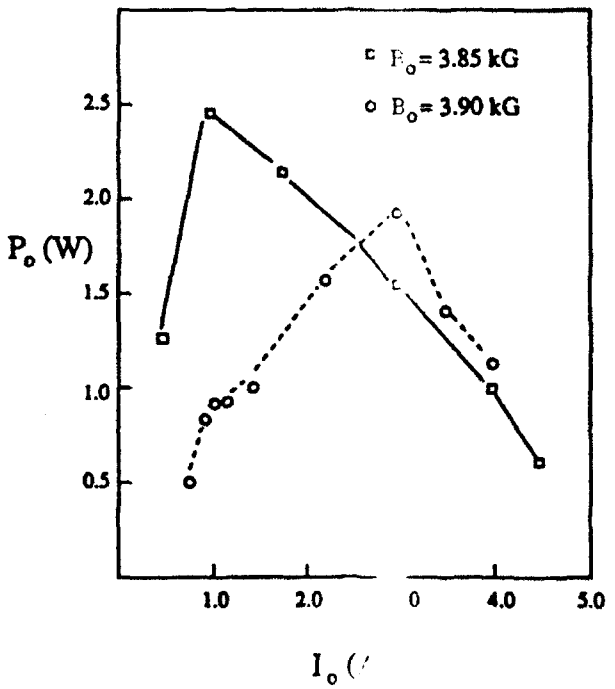

Figure 4. Dependence of out power on beam current.

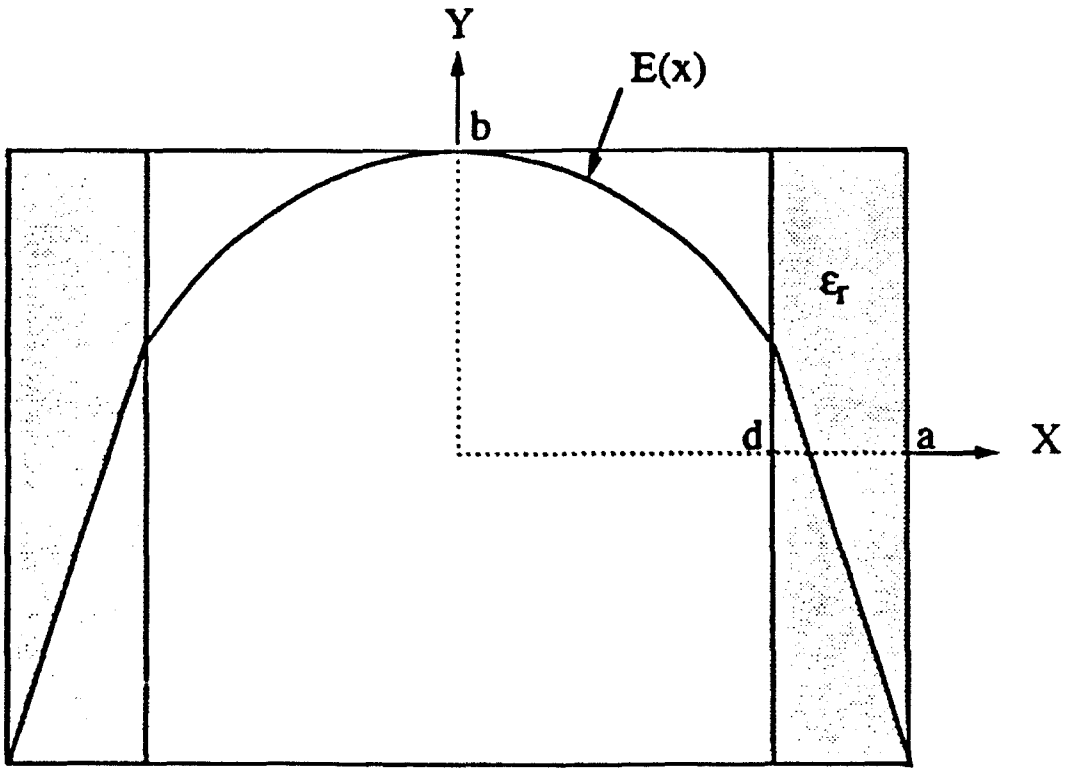

Figure 5. Cross sectional view of dielectric loaded rectangular waveguide. Dashed line represents typical electrical field profile.

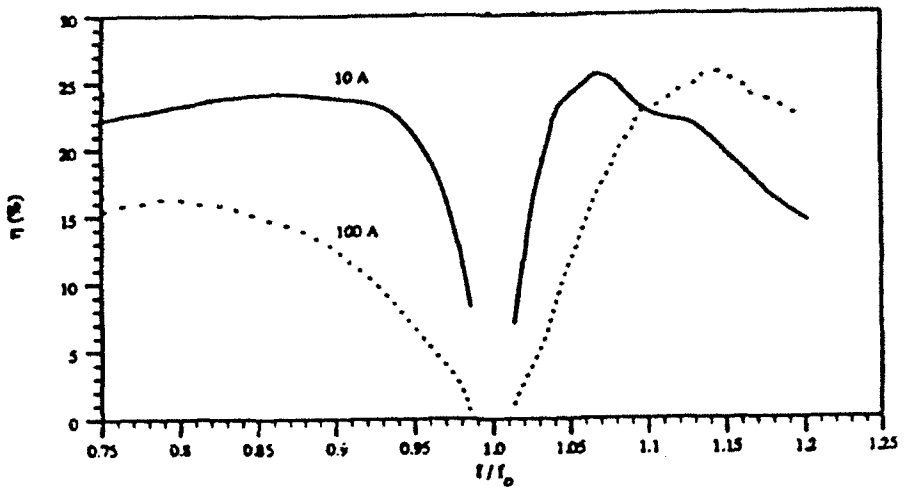

(a)

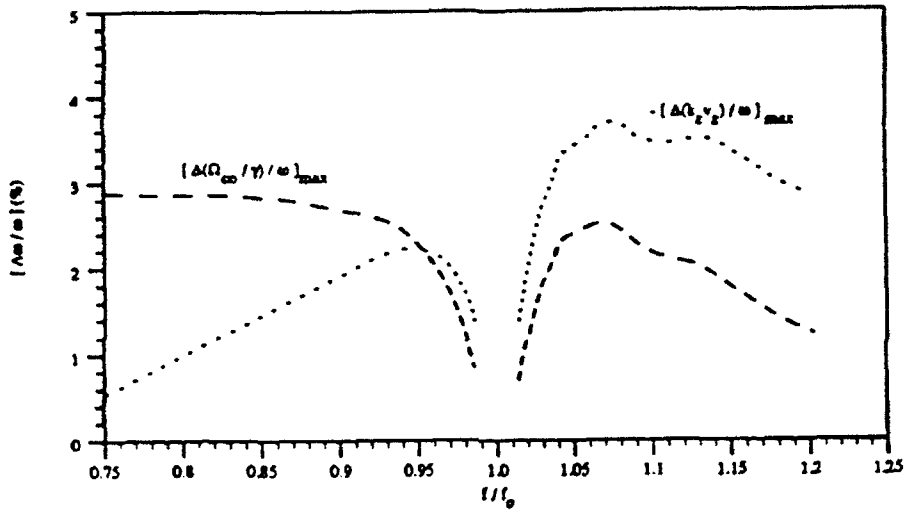

(b)

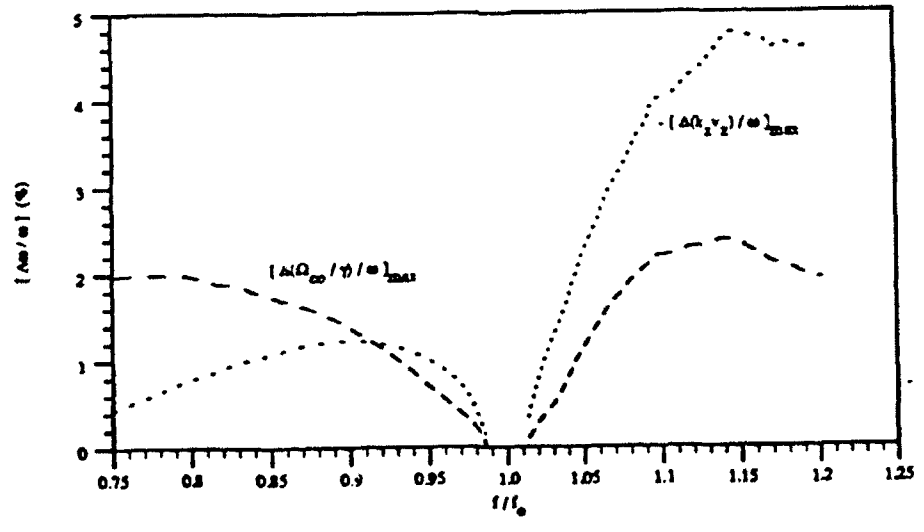

(c)

Figure 6. (a) Dependence of efficiency on frequency normalized to the frequency at which $\omega/ck_{\|} = 1$ for two values of beam current. The variance of relativistic gyrofrequency and Doppler shift for (b) I = 10 A and (c) I = 100 A. ($\omega_c = 1.57$, $\epsilon = 9.67$, b/a = 0.75, d/a = 0.75, $v_o = 100$ kV, $\Delta = 0.0$, $\alpha = 1.0$, $\Delta v_z/v_z = 0.0\%$.)

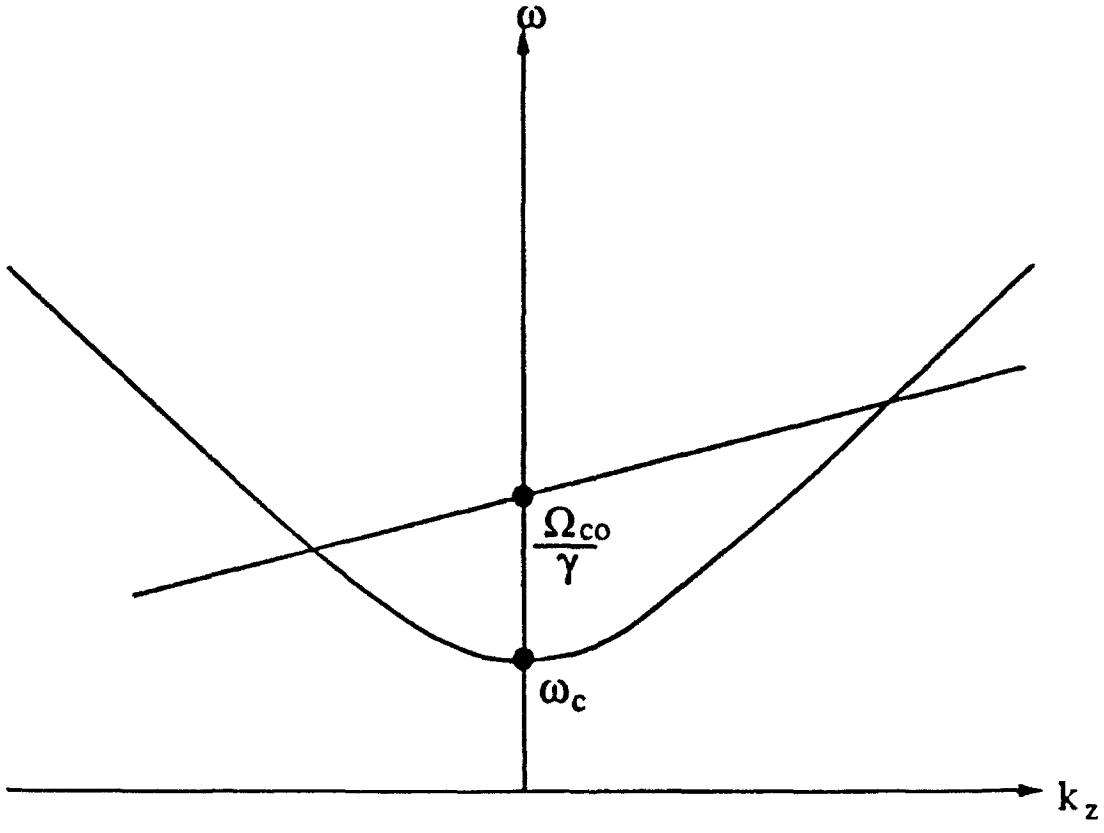

Figure 7. Uncoupled dispersion diagram of gyro-TWT with an elevated magnetic field showing the intersection of the gyroresonance line with a fast waveguide mode.

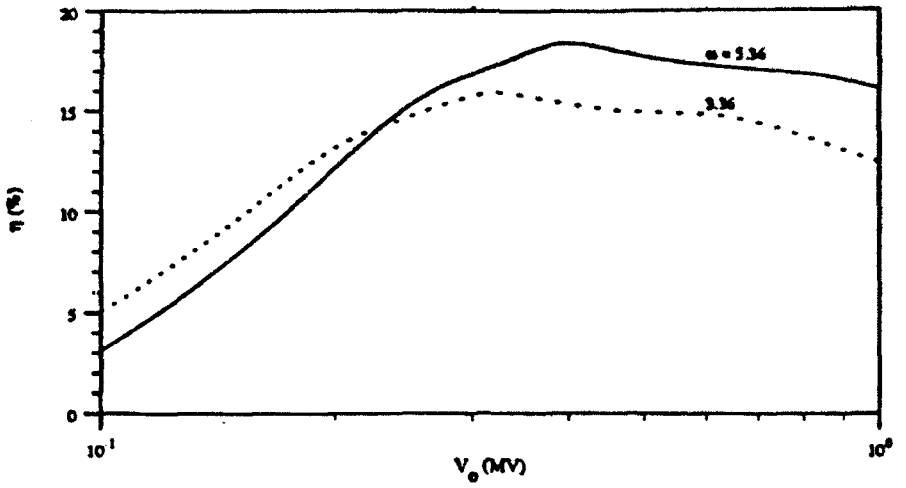

(a)

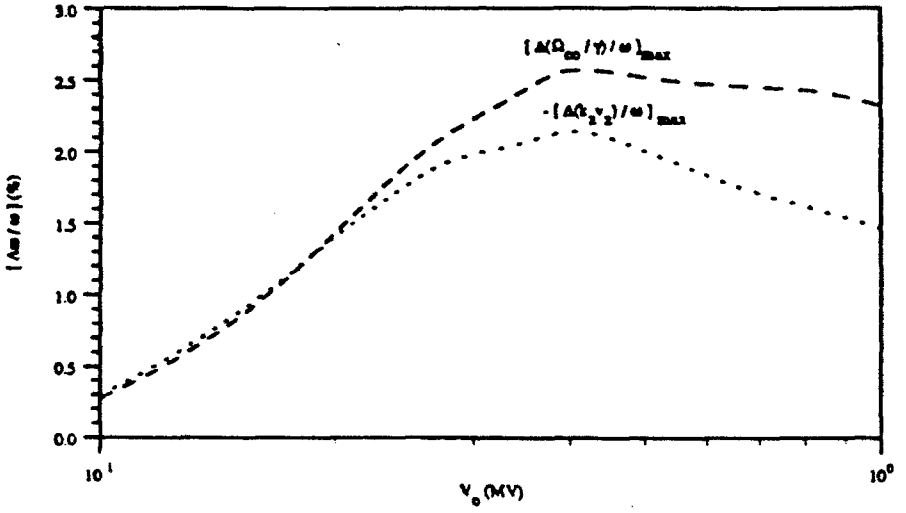

(b)

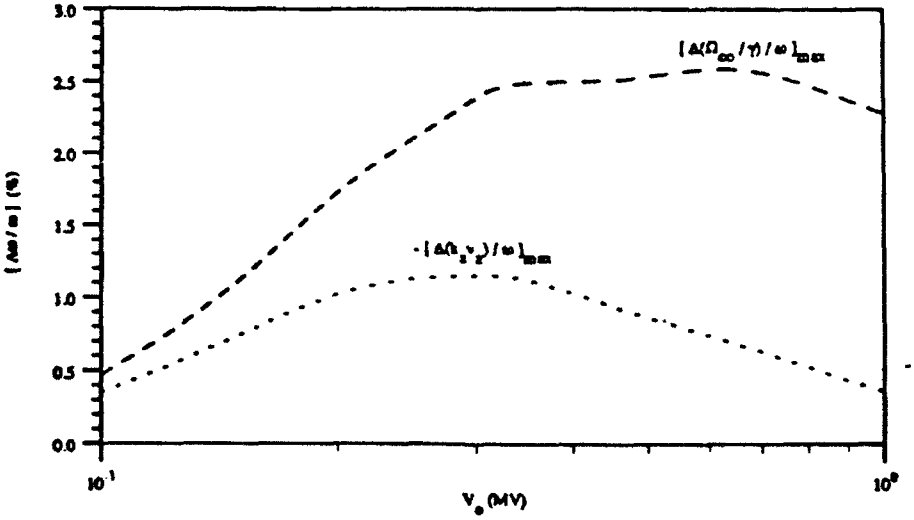

(c)

Figure 8. (a) Dependence of efficiency on beam voltage for $\alpha = 0.5$ and two values of frequency. The variance of relativistic gyrofrequency and Doppler shift for (b) $\omega = 5.36$ and (c) $\omega = 3.36$. ($\omega_c = 1.57$, $I_o = 50$ A, $P_{\text{in}} = 1$ kW, $\Delta = 0.0$, $\Delta V_z/v_z = 0.0\%$.)

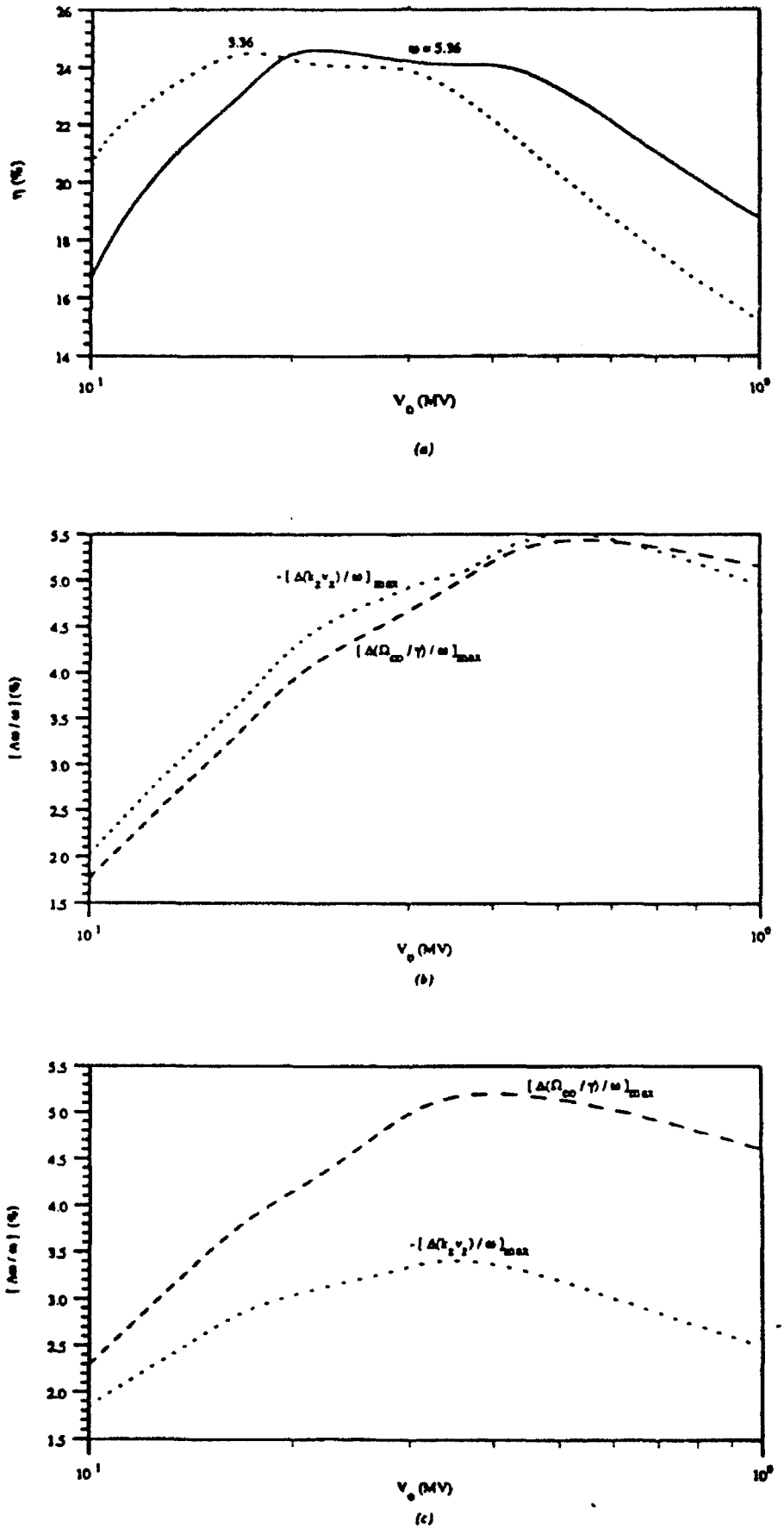

Figure 9. (a) Dependence of efficiency on beam voltage for $\alpha = 1.0$ and two values of frequency. The variance of relativistic gyrofrequency and Doppler shift for (b) $\omega = 5.36$ and (c) $\omega = 3.36$. ($\omega_c = 1.57$, $I_o = 50$ A, $P_{in} = 1$ kW, $\Delta = 0.0$, $\Delta v_z/v_z = 0.0\%$.)

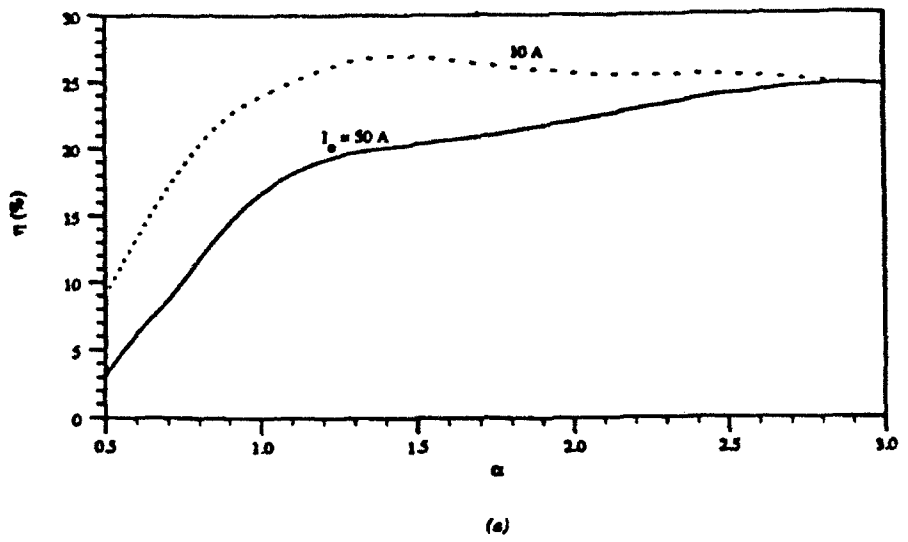

(a)

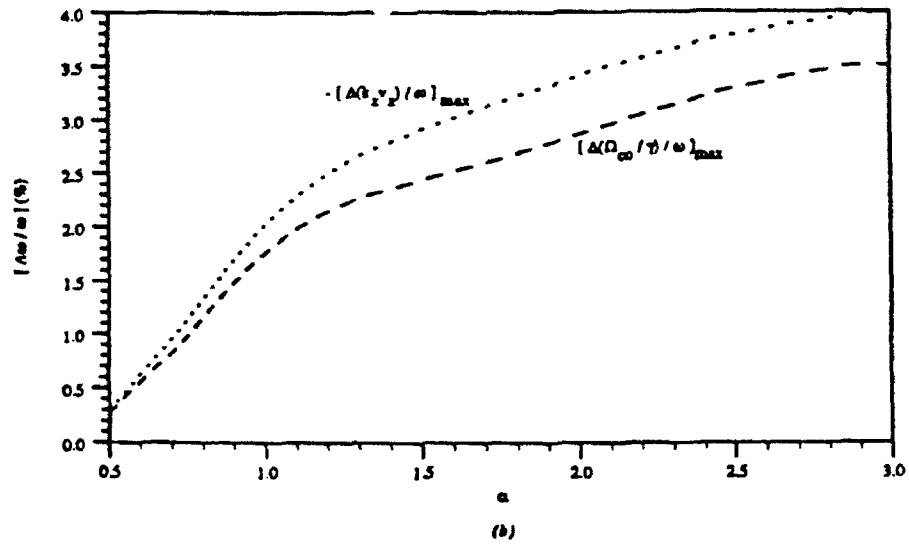

(b)

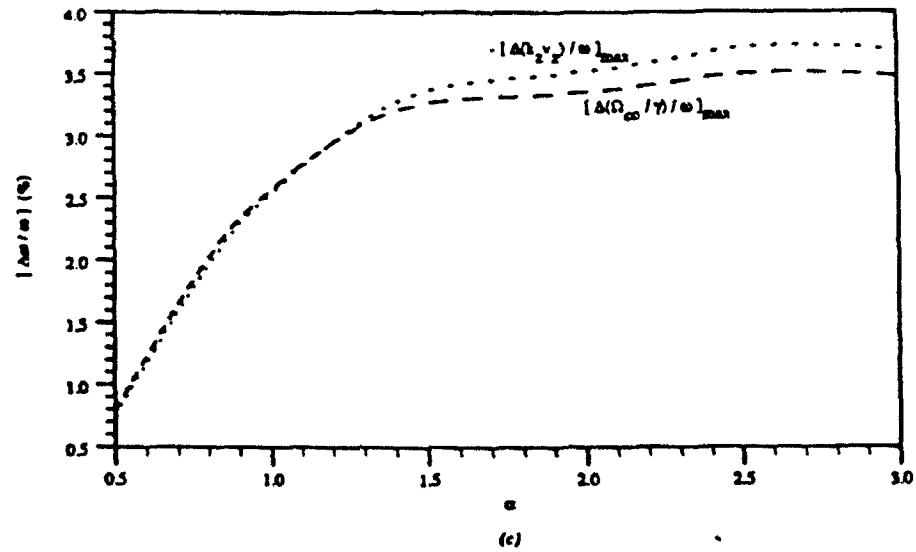

(c)

Figure 10. (a) Dependence of efficiency on $\alpha(= v_\perp/v_{||})$ for two values of beam current. The variance of relativistic gyrofrequency and Doppler shift for (b) I_o = 50 A and (c) I_o = 10 A. (ω_c = 1.57, V_o = 100 kV, ω = 5.36, Δ = 0.0, $\Delta v_z/v_z$ = 0.0%.)

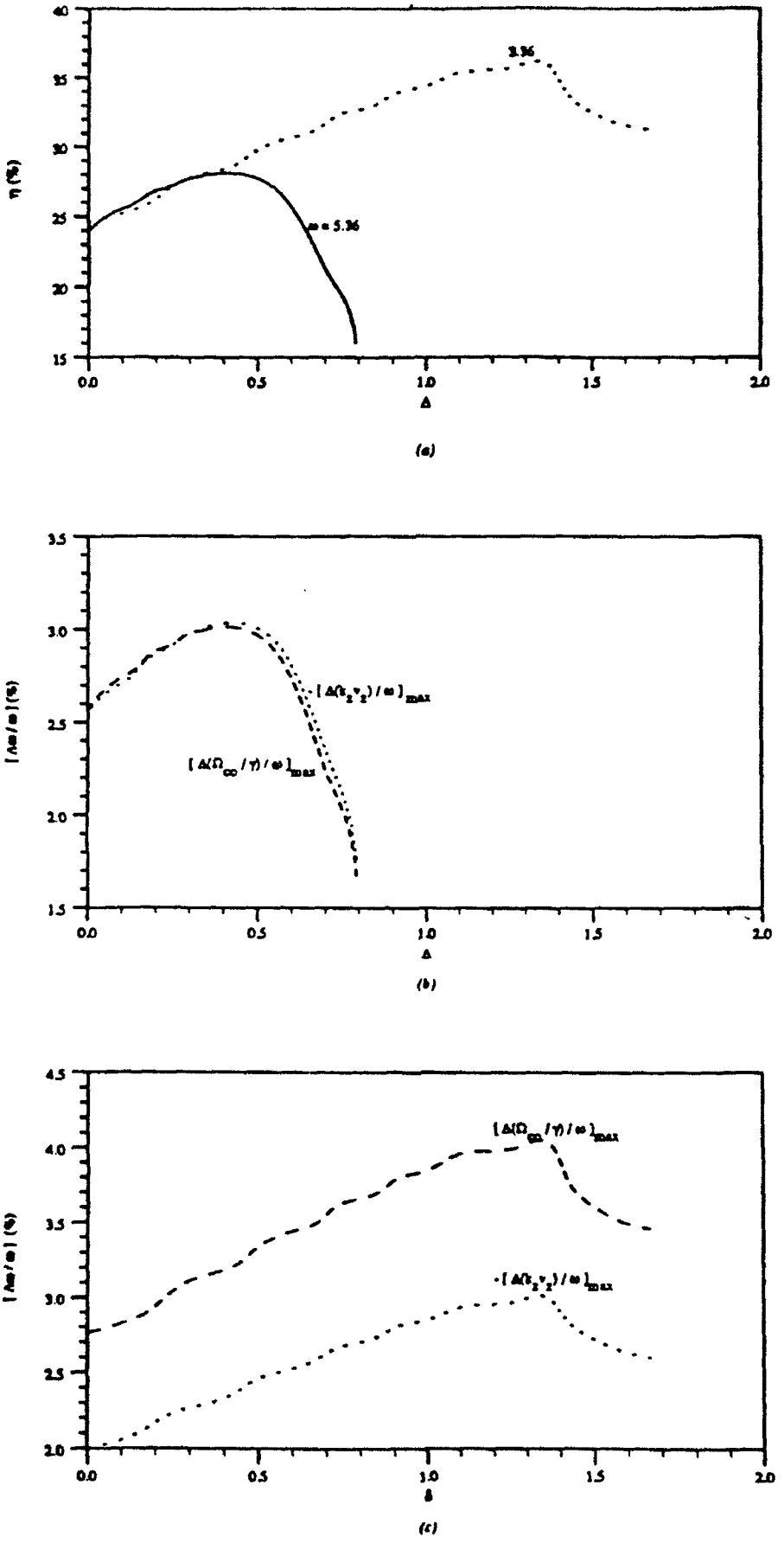

Figure 11. (a) Dependence of efficiency on mismatch ($\Delta = (\omega - \Omega_c - k_z v_z)/\omega$) for two values of frequency. Variance of gyrofrequency and Doppler shift for (b) $\omega = 5.36$ and (c) $\omega = 3.36$. ($\omega_c = 1.57$, $V_o = 100$ kV, $I_o = 10$ A, $\alpha = 1.0$, $\Delta v_z/v_z = 0.0\%$, $P_{in} = 100$ W.)

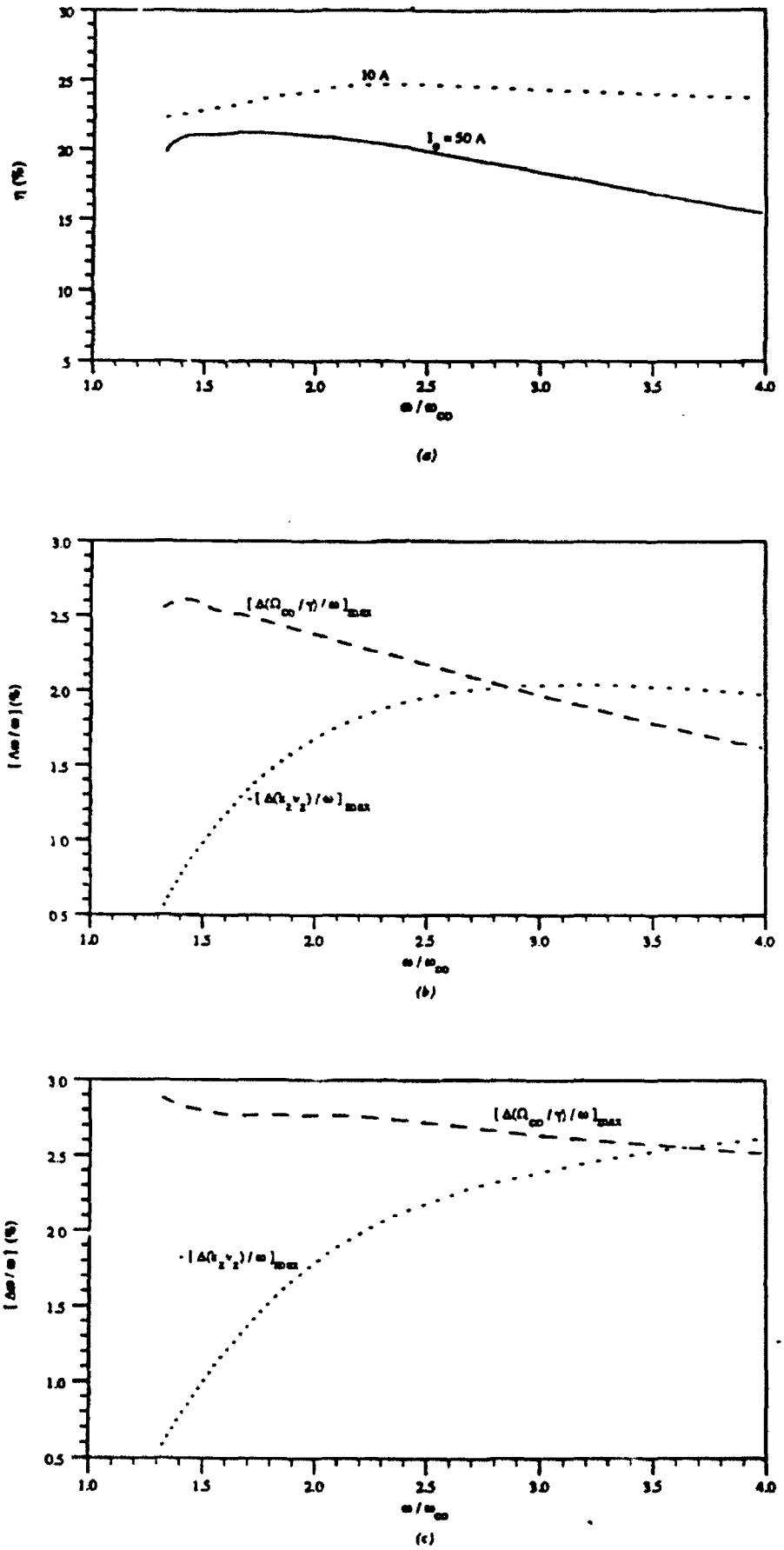

Figure 12. (a) Dependence of efficiency on frequency normalized to the cutoff frequency for two values of beam current. Variance of gyrofrequency and Doppler shift for (b) $I_o = 50$ A and (c) $I_o = 10$ A ($\omega_c = 1.57$, $V_o = 100$ kV, $\alpha = 1.0$, $\Delta = 0.0$, $\Delta v_z/v_z = 0.0\%$.)

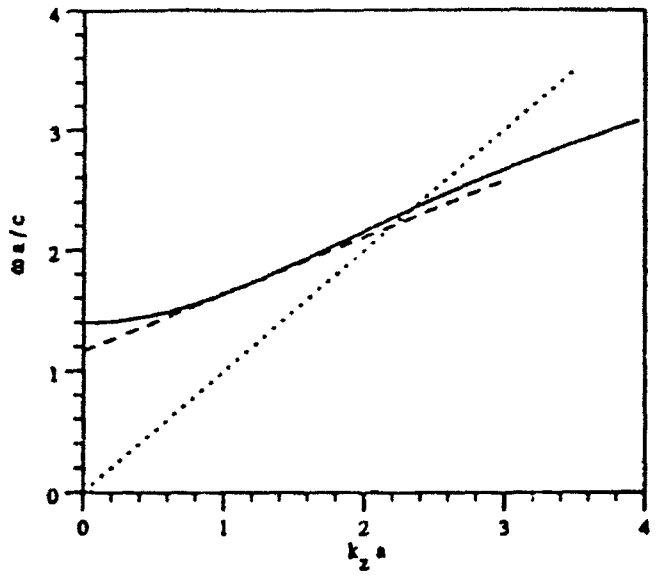

Figure 13. Dispersion of dielectric loaded waveguide (solid line), cyclotron resonance line (dashed line) and vacuum light line (dotted line).

Beam Voltage	100 kV
Beam Current	5 A
Center Frequency	33 GHz
Instantaneous Bandwidth	20 %
Output Power	40 - 80 kW
Gain	26-29 dB
Magnetic Field	9.35 kG
$v_\perp/v_z$	0.59
$\Delta v_z/v_z$	2.0 %
Interaction Length	30 cm
Waveguide Width	5.0 mm
Waveguide Height	3.5 mm
Dielectric Thickness	0.75 mm
Dielectric Constant	6.0

Table 1. Parameters for Proposed Dielectric Loaded Broadband Ka-band Gyro-TWT.

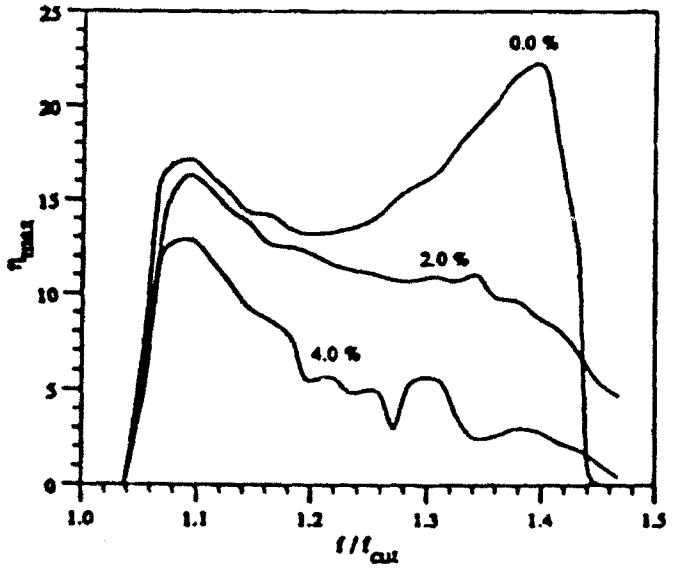

Figure 14. Dependence of saturation efficiency on frequency for several values of axial velocity spread for parameters listed in Table 1, except length is variable.

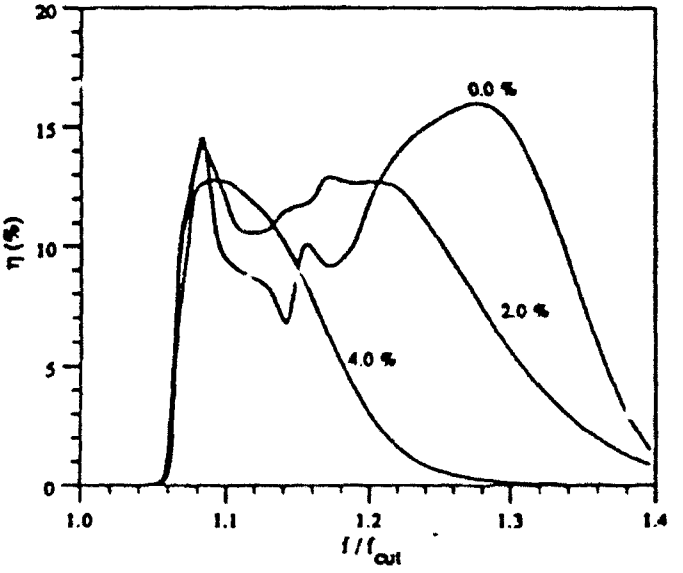

Figure 15. Dependence of instantaneous efficiency on frequency for several values of axial velocity spread for fixed parameters listed in Table 1.

Table 2. Parameters of Magnetron Injection Gun with Single Anode for X-Band Dielectric Loaded Wideband Gyro-TWT.

Voltage	100 kV
Current	5 A
Current Density	6.75 A/cm^2
Angle of Emitting Surface	67°
Emitting Strip Radius	4.30 mm
Emitting Strip Length	2.63 mm
Cathode Anode Distance	3.53 cm
Magnetic Compression Ratio	4.5
Velocity Ratio	0.59
Axial velocity Spread	2.0 %
Guiding Center Spread	32 %

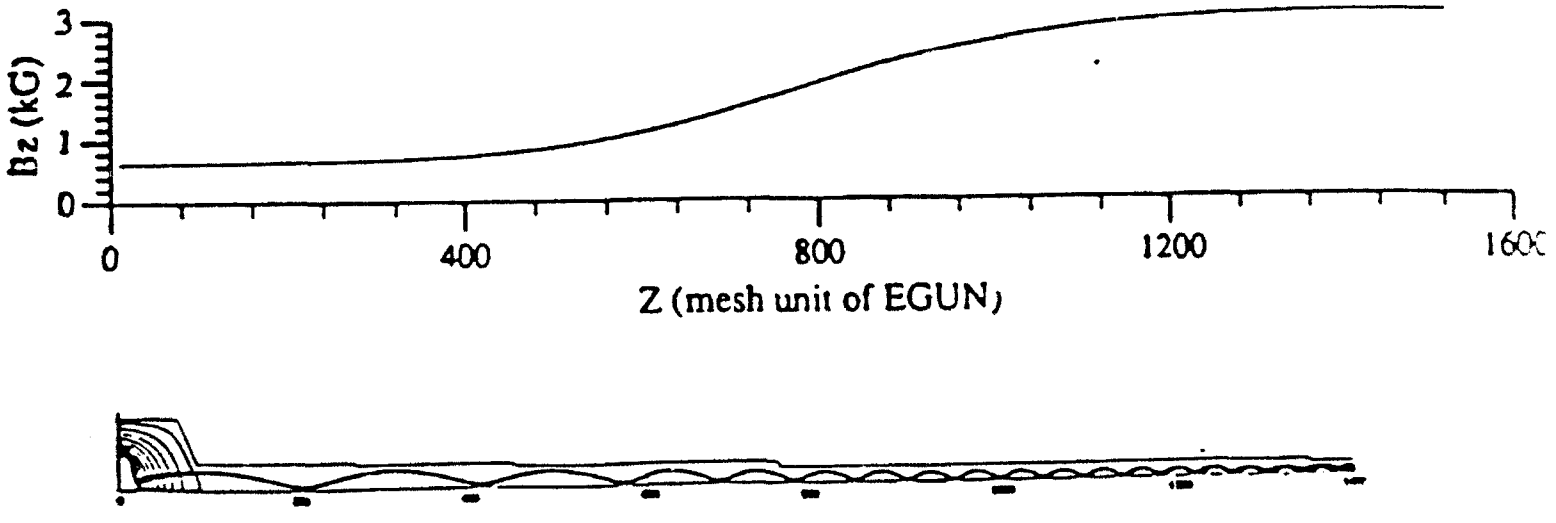

Figure 16. Magnetic field profile and trajectories of electron beam from single anode magnetron injection gun as predicted by EGUN

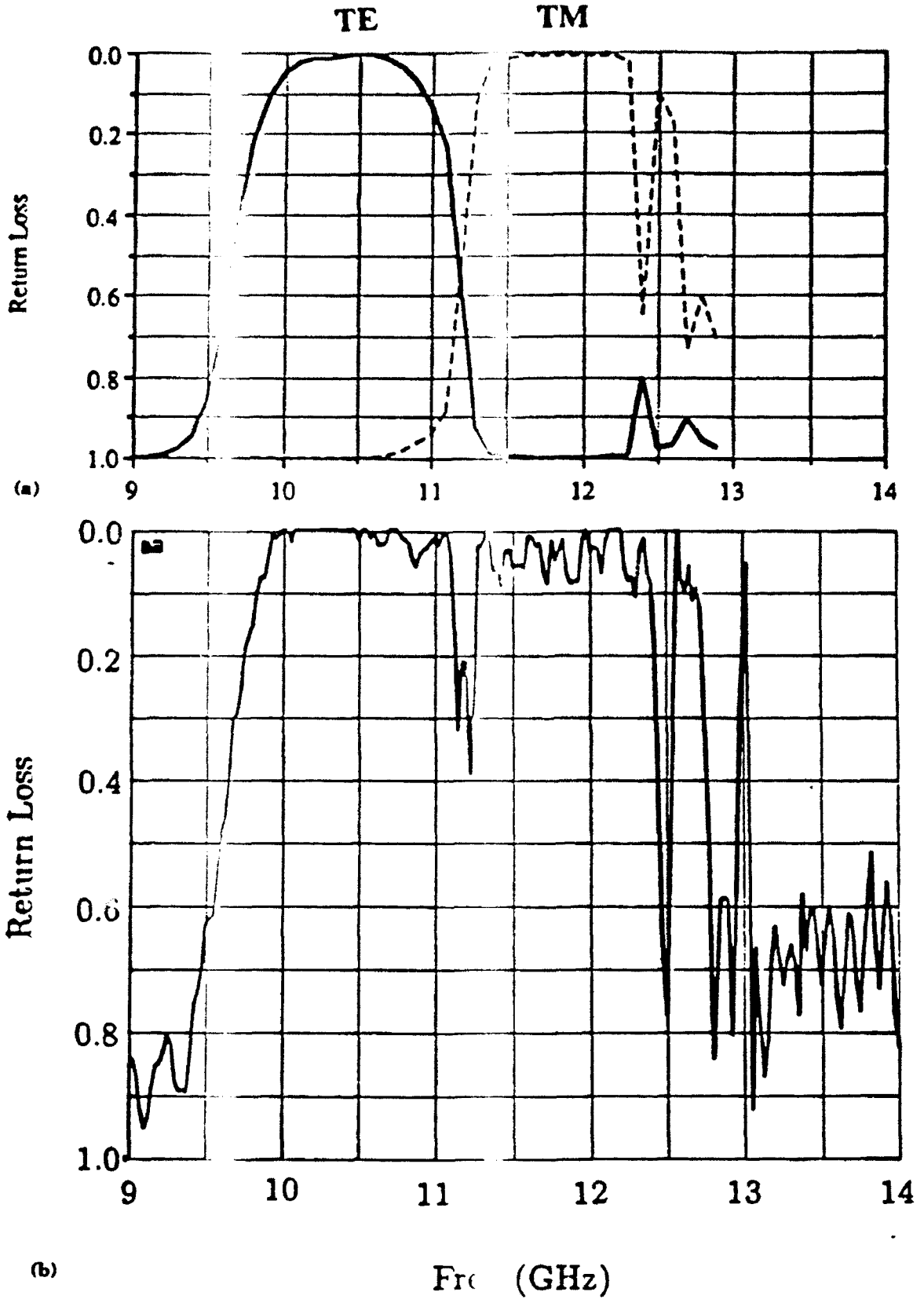

Figure 17. F ency dependence of TE_{11} d TM_{11} mode reflection from a single Hamming-Window refl with a peak corrugati mplitude of 0.40 cm from (a) scattering matrix simulation b) measurement. The t wave is in the TE_{11} mode.

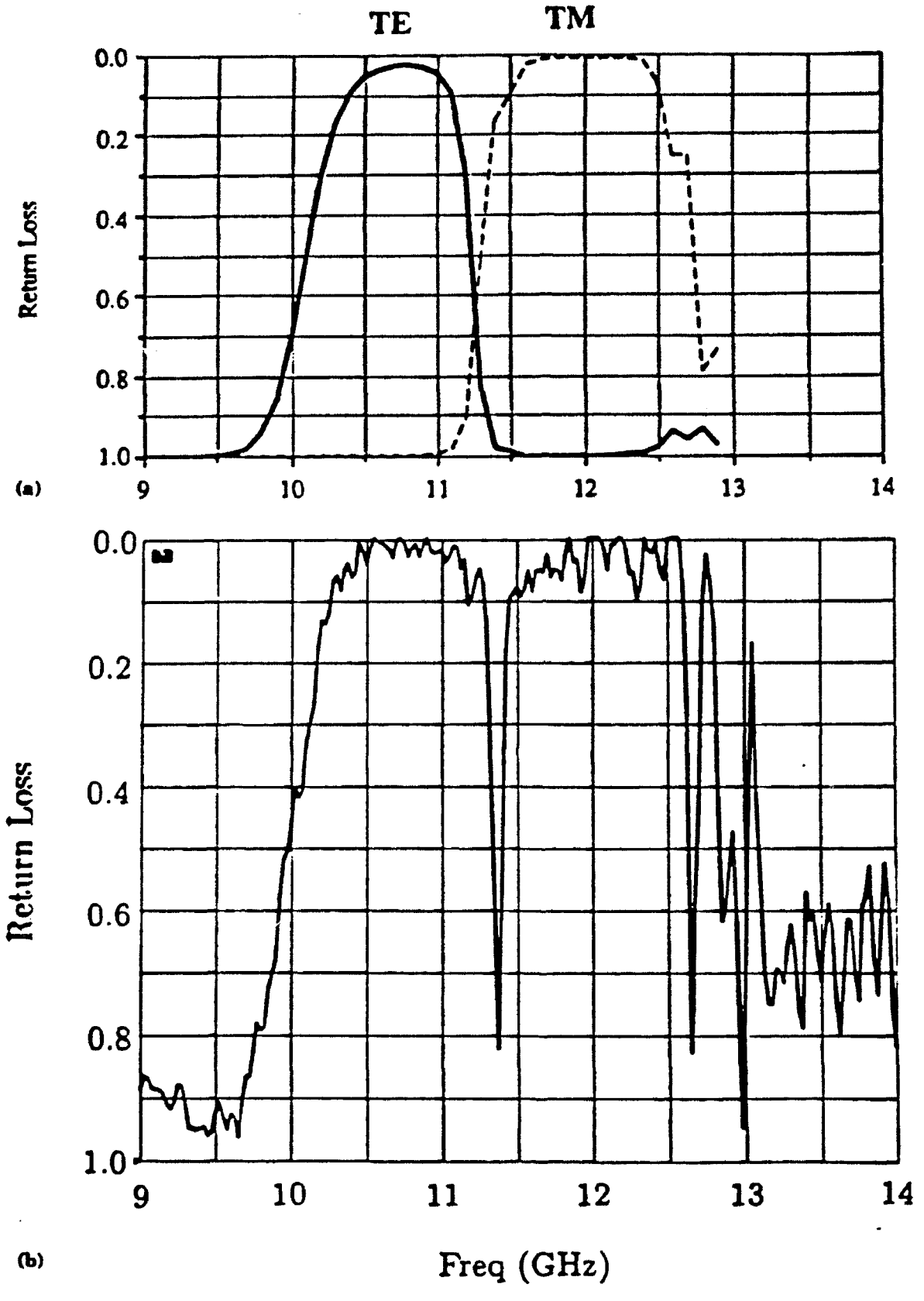

Figure 18. Frequency dependence of TE_{11} and TM_{11} mode reflection from a single Hamming-Window reflector with a peak corrugation amplitude of 0.325 cm from (a) scattering matrix simulation and (b) measurement. The input is in the TE_{11} mode.

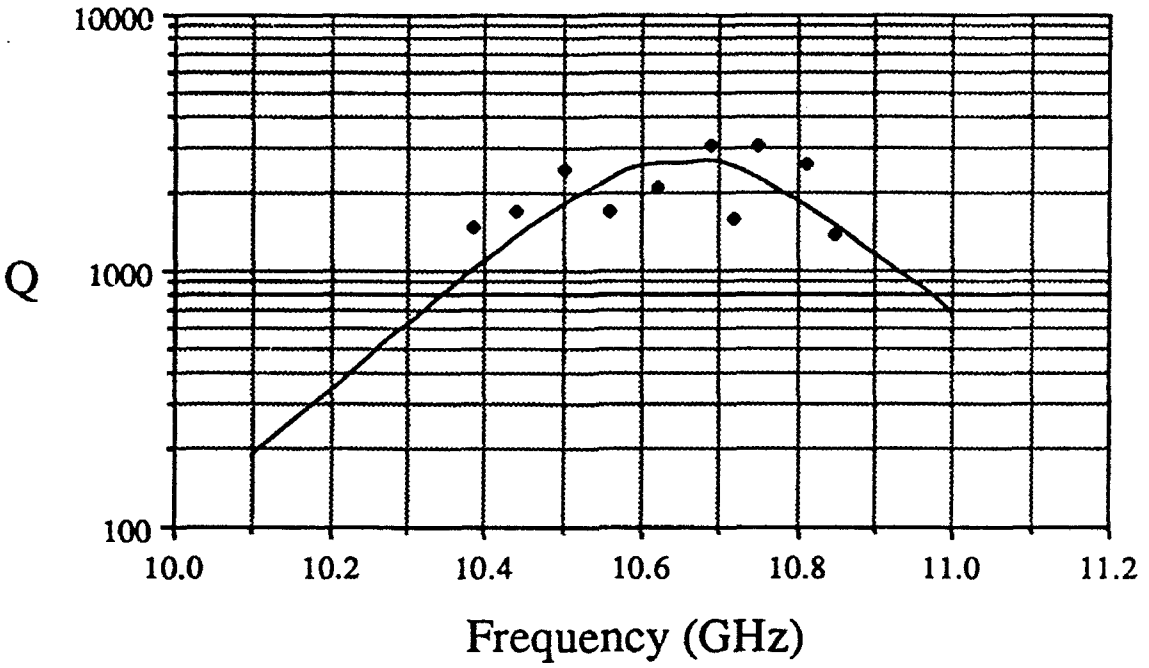

Figure 19. Theoretical and measured dependence of quality factor of Bragg resonator comprised of a 23.5 cm smooth section and the two Hamming-Window reflectors described in Figs. 17 and 18.

Table 3. Parameters for Proposed Negative Energy CRM Proof of Principle Experiment.

Beam Voltage	511 kV
Beam Current	68 A
Efficiency	27%
Frequency	9.3 GHz
Bandwidth	7%
Magnetic Field	3.6 kG
$\Delta v_\perp / v_\parallel$	2.5 %
Beam Radius	0.22 cm
Waveguide Broad Wall	1.2 cm
Waveguide Narrow Wall	0.436 cm
Dielectric Slab Thickness	0.382 cm
Dielectric Constant, ϵ	12

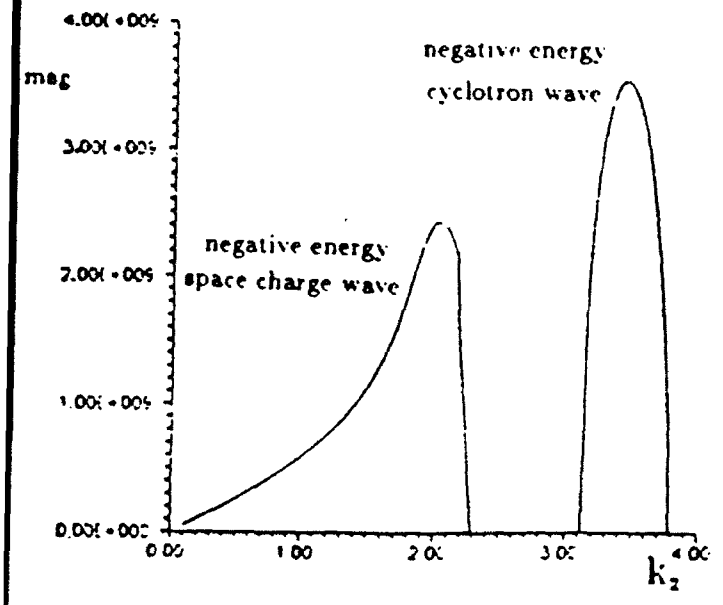

Figure 20. Dependence of growth rate on axial wavevector of negative energy cyclotron wave (SWCM) and space charge wave (SWCM) for proposed experiment described in Table 3, but with cold electron beam. ($\gamma = 2$, $\epsilon = 12$, $B_o = 3.6$ kG, and $\omega_p = 10^{10}$ rad /sec.

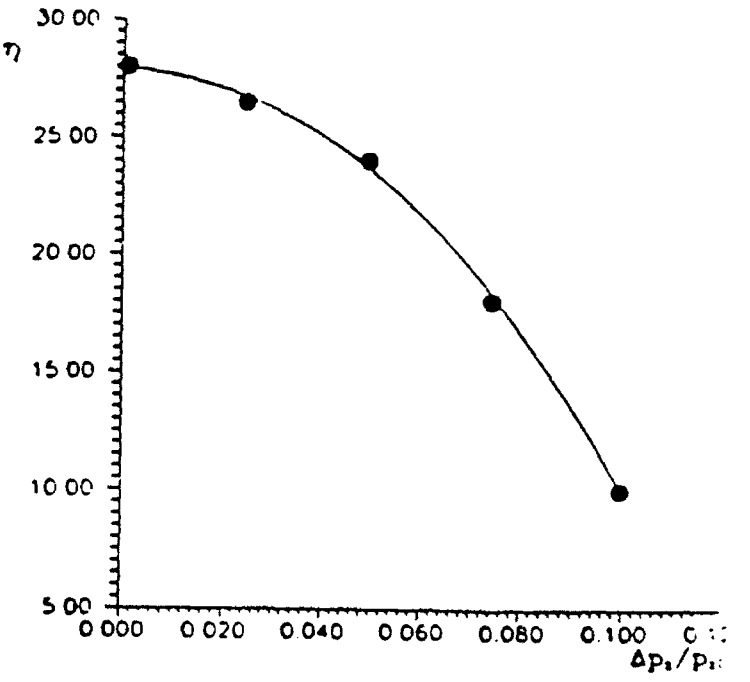

Figure 21. Dependence of efficiency from simulation for the proposed Negative Energy CRM proof of principle experiment described in Table 3.